J. Phys. B: At. Mol. Opt. Phys. **42** (2009) 235701 (11pp) doi:10.1088/0953-4075/42/23/235701

Radiative opacities of hot and solid-dense aluminium plasmas using a detailed level accounting model

Yongqiang Li, Jianhua Wu, Yong Hou and Jianmin Yuan[1]

Department of Physics, National University of Defense Technology, Changsha 410073, People's Republic of China

Received 1 June 2009, in final form 16 October 2009
Published 23 November 2009
Online at stacks.iop.org/JPhysB/42/235701

Abstract

An approach based on the self-consistent-field (SCF) multi-configuration Dirac–Fock (MCDF) model is developed to simulate radiative opacity of hot and solid-dense plasmas taking detailed levels into account. The correlation effects and the angular momentum coupling among the bound electrons are treated in the usual way employed in a normal MCDF method. Influences of plasma screening on transition energies, oscillator strengths and ionization potentials are included by introducing a correction to the one-electron potential to account for the screening of the ionized electrons. This correction depends on the detailed micro-space distribution of the ionized electrons in different ions. The total average number density of the ionized electrons in the plasma is obtained by solving the Saha equation with quantum degeneracy corrections. The ionized electron density distribution in each ion is described based on a Thomas–Fermi distribution in an atomic field. Since the electronic structure and the ionization balance depend on each other, the SCF procedure includes solving the MCDF and the Saha equations. As examples, calculations have been carried out to simulate the spectrally resolved radiative opacity and the Rosseland and Planck means of hot and solid-dense aluminium plasmas. Comparisons between the results of the present model, average atom model and experiments are made to show the significance of detailed line-by-line treatments on the calculated results.

(Some figures in this article are in colour only in the electronic version)

1. Introduction

Opacity dominates the radiative transfer within plasmas and consequently has a strong influence on radiative hydrodynamic evolutions. It is of great significance in many research fields such as astrophysical plasmas [1], inertial confinement fusion (ICF) [2] and x-ray lasers. In the past few decades, extensive studies on the opacity of plasmas with temperatures of a few tenths of eV and densities of two orders less than solids have been done both experimentally and theoretically [3–8]. Only recently, however, have experiments been performed to investigate the properties of hot and solid-dense plasmas due to the technical advances in generating near or above solid-dense plasmas [9–21]. As for the theoretical methods, opacity of hot and dense plasmas has sufficient complexity to be reasonably approximated by statistical models such as the average atom (AA) model [22–25], super transition array (STA) model [26, 27] and unresolved transition array (UTA) model [28] with a variety of considerations for the plasma environment. Few detailed term/level accounting (DTA/DLA) models [4, 5] have been applied to simulate radiative opacity of hot and solid-dense plasmas. However, many theoretical models [29–44] have been developed to calculate the atomic data in this kind of plasmas.

For low-density plasmas, a large number of atomic data, such as the atomic levels, level populations, oscillator strengths and photoionization cross section, are used with the same values as those of the free ions without environmental influence except that the ionization potential depression is usually taken into account by simple models [29, 30]. For solid-dense plasmas, influence of the plasma environment should be

[1] Author to whom any correspondence should be addressed.

 © 2009 IOP Publishing Ltd Printed in the UK

considered in the calculation of atomic data along with the calculation of ionization balance of ions in the plasma. Except for the well-developed AA models [22–25], most recently, quantum mechanical description of an ionized electron had been included in an improved STA model by using partial wave expansion [26, 27]. Local density approximation (LDA) potential was connected with the STA optimized parametric potentials allowing for bound orbital relaxation. Description for the pressure-induced ionization process of electrons across the ionization threshold with increase of matter density had been improved by including shape resonance orbitals just above the ionization threshold. However, in the latest versions of the DTA/DLA models [4–6], calculations of the bound electron structure have not been coupled with plasma, although the ionized electrons as well as the ionization balance are treated in a relatively complete way.

In the present study, a DTA/DLA model is developed for opacity calculations of hot and dense plasmas by coupling a modified multi-configuration Dirac–Fock (MCDF) scheme for bound electron calculations with ionized electrons and ionization balance of plasma self-consistently. A flexible MCDF code GRASP2 [45, 46], which is capable of calculating the electron correlation effects as well as the angular momentum coupling, has been modified to take the effect of ionized electron screening as well as finite space confinements for bound electrons into account. The changes of energy levels, oscillator strengths and ionization potential of the ions along with plasma temperature and density have been considered automatically during the self-consistent calculation of atomic data and the ionization balance of plasma. As an example, the opacity of hot and solid-dense Al plasmas is calculated using this model. Changes of the fine spectrally resolved radiative absorption structures and Rosseland and Planck mean opacities with density and temperature are investigated for a wide range of plasma conditions with a density of 0.2–20 g cm^{-3} and a temperature of 300–500 eV, respectively. Preliminary experimental results are available within this range of density and temperature [12, 13].

Experimental measurement of opacity will soon be possible for hot and solid dense matters when new devices such as NIF [19] will be ready to use. Therefore, accurately calculated opacity will be interesting for many researches in the field such as ICF. Although opacity can be obtained by summing all cross sections of radiative absorption and scattering processes together, many important features such as the widths and strengths of absorption bands caused by transition arrays cannot be deduced from the atomic data. These features are essential for people to design the experiment and make practical applications in ICF simulations. Therefore, the main purpose of the present study is not only to show the density effect on atomic data but also to give quantitatively accurate opacity results for hot and solid-dense plasmas, which would be valuable for the physics experiment design on new devices and for the possible comparison between experiment and theory.

2. Method of calculation

Calculation of opacity of hot and solid-dense plasmas requires massive amounts of accurate environmental dependent atomic data, ion abundance and energy level populations. Atomic data are obtained with a modified MCDF approach with environmental effects being considered. Ion and energy level populations are obtained with a local thermodynamic equilibrium (LTE) approximation. Brief descriptions of the method are given in the following.

2.1. Modified MCDF method

In the MCDF approach, an atomic state function (ASF) is constructed approximately by a linear combination of configuration state functions (CSFs) with the same parity P and angular momentum (J, M)

$$|\Gamma PJM\rangle = \sum_{r=1}^{n_c} c_{r\tau} |\gamma_r PJM\rangle, \tag{1}$$

where n_c is the number of CSFs and $c_{r\tau}$ is the mixing coefficient. A CSF is antisymmetrized products of a common set of orthonormal orbitals which are optimized on the basis of the relativistic Hamiltonian. For free ions, the Hamiltonian takes the form

$$H_0 = \sum_i [c\alpha \cdot \mathbf{p} + \beta c^2 + V_{\rm nuc}(r_i)] + \sum_{i>j} \frac{1}{r_{ij}}, \tag{2}$$

where c is the speed of light in vacuum and $V_{\rm nuc}(r_i)$ is the potential due to the nucleus. The Hamiltonian for the ions in the plasma environment is of the same basic form as that for free ions

$$H_e = \sum_i [c\alpha \cdot \mathbf{p} + \beta c^2 + V_e(\mathbf{r}_i)] + \sum_{i>j} \frac{1}{r_{ij}}, \tag{3}$$

except that the potential $V_{\rm nuc}(r_i)$ due to the nucleus is replaced by the potential $V_e(\mathbf{r}_i)$ due to the nucleus and the ionized electrons. In the central field approximation, for the Ith ion in the plasma with a finite radius of $R_I = \left[3\left(Z - N_b^I\right)/(4\pi N_e)\right]^{1/3}$, the potential is given by

$$V_e(r_i) = V_{\rm nuc}(r_i) + 4\pi \left[\frac{1}{r_i}\int_0^{r_i} r_1 + \int_{r_i}^{R_I}\right] r_1 \rho_f^I(r_1)\, {\rm d}r_1, \tag{4}$$

where Z, N_b^I, N_e and $\rho_f^I(r)$ are the nuclear charge, number of bound electrons of the Ith ion, average ionized electron number density in the plasma, and the ionized electron density distribution in the ion-sphere of the Ith ion, respectively. The ionized electrons are considered to follow the Fermi–Dirac distribution of the local free electron gas in the plane wave momentum κ space [25] and can be defined as

$$\rho_f^I(r) = \frac{1}{\pi^2}\int_{\kappa_0(r)}^{\infty} \frac{\kappa^2\, {\rm d}\kappa}{{\rm e}^{[\sqrt{\kappa^2c^2+c^4}-c^2-V(r)-\mu_I]/kT}+1}, \tag{5}$$

where $\kappa_0(r) = [2V(r)c^2 + V(r)^2]^{\frac{1}{2}}$ and μ_I is the so-called chemical potential. The chemical potential is determined by the neutrality condition

$$4\pi \int_0^{R_I} r^2 \rho_f^I(r)\, {\rm d}r = Z - N_b^I. \tag{6}$$

One can see that different ions have different radii of ion-sphere. The higher the ionization stage of the ion, the larger the corresponding ion-sphere. The charge neutrality is satisfied not only on average but also for every ion. Therefore, this ion-sphere could not be understood as the average bound electron distribution region as people usually do for ions in crystal, but as the region in which the ionized electrons are influenced by this ion. This treatment for electron space distribution was widely used in Thomas–Fermi [47] and average atom models [22, 23, 25] for electronic structure calculations in atoms, solids and dense plasmas. It describes the true electron distributions much better than the very simplified uniform ion-sphere model [41]. For a neutral atom, $R_I = [3/(4\pi N_e)]^{1/3}$ is taken just as the ion-sphere radius to calculate the wavefunction but not to calculate the free electron distribution.

Once gotten the total Hamiltonian including the contributions from the ionized electrons in the sphere, the environmental-dependent single-electron orbital is obtained just as before by solving the one-electron equation similar to (2) except for the boundary conditions, where the radial components of the wavefunction $P_a(r)$ and $Q_a(r)$ for bound states are assumed to satisfy

$$P_a(R_I) = 0 \qquad \text{or} \qquad \left.\frac{\mathrm{d}P_a(r)}{\mathrm{d}r}\right|_{r=R_I} = 0. \tag{7}$$

Details of the bound electron wavefunction calculations were described elsewhere [42]. In a plasma consisting of many different ionized ions, the relative abundance of the ions and the average ionized electron number density depend on the density and temperature of the plasma. The method of determining N_e and the percentage of different ions will be described in the following section. It will be seen that the distribution of the energy levels and ionization thresholds obtained in this section are required to get N_e and the relative abundance of the ions. Therefore, for the plasma with definite density and temperature, atomic structure and the ionization balance of the plasma are calculated in a whole self-consistent way in the present study. However, the ion–ion dynamical correlation [12, 38, 43, 44] has not been considered in the present and other similar static ion-sphere models.

2.2. *Radiative opacity in solid-dense aluminium plasma*

In the case of the local thermodynamic equilibrium (LTE), the radiative opacity κ_v [3] at radiation with energy hv in a plasma is

$$\rho\kappa_v = \sum_I \left[\sum_{ll'} N_{Il}\sigma_{Ill'}(hv) + \sum_l N_{Il}\sigma_{I\alpha}(hv) + \mu_{ff}(hv)\right] \times (1 - \exp^{-hv/kT}) + \mu_s, \tag{8}$$

where κ_v is the opacity at the energy hv, ρ is the density of the plasma, T is the temperature, $\sigma_{Ill'}$ is the cross section for the photoexcitation from level l to l' of ion I, $\sigma_{I\alpha}$ is the total cross section for the photoionization from level l of ion I, μ_{ff} is the total free–free absorption coefficient and μ_s is the total photon scattering coefficient by free electrons.

The photoexcitation cross section from level l to l' can be expressed in terms of the oscillator strength $f_{ll'}$ as

$$\sigma_{Ill'}(hv) = \frac{\pi he^2}{m_e c} f_{Ill'} S(hv), \tag{9}$$

where $S(hv)$ is the line shape function, which is taken as a Voigt profile with the line widths of Doppler and Stark broadening considered. The Stark width was obtained from a simplified semi-empirical method [48]. The photoionization cross section from level l of ion i is obtained from

$$\sigma_{Il}(hv) = \frac{\pi he^2}{m_e c}\frac{\mathrm{d}f_{Il\epsilon}}{\mathrm{d}(hv)}, \tag{10}$$

where $\mathrm{d}f_{Il\epsilon}/\mathrm{d}\epsilon$ is the photoionization oscillator strength density per photon energy interval. Equations (9) and (10) are calculated with fully relativistic forms. The free–free absorption is obtained from the Kramers cross section, and the scattering contribution is approximated using the Thomson scattering cross section.

In the LTE plasma, N_{Il}, the population density for level l of ion stage I, is obtained from the Boltzmann distribution function

$$N_{Il} = g_{Il}(N_I/Z_I)\,\mathrm{e}^{-E_{Il}/kT}, \tag{11}$$

where g_{Il} is the degeneracy of the state l. N_I, the total population density of ion I, is determined by solving the Saha equation [49–51]

$$\frac{N_{I+1}N_e}{N_I} = \frac{Z_{I+1}Z_e}{Z_I}\,\mathrm{e}^{-\phi_I/kT}, \tag{12}$$

where N_e is the number of ionized electrons per unit volume, ϕ_I is the density and temperature-dependent ground-state ionization potential of ion I, and Z_I and Z_e are the partition functions for ion I and free electron, respectively. For nondegenerate gases, they are

$$Z_I = \sum_l g_{Il}\,\mathrm{e}^{-E_{Il}/kT} \tag{13}$$

and

$$Z_e = 2\left(\frac{2\pi m_e kT}{h^2}\right)^{3/2}, \tag{14}$$

respectively, where E_{Il} is the energy of level l relative to the ground state of ion I and $g_{Il} = 2J_l+1$ is the degeneracy of level l. The sum of equation (13) runs over all bound states of ion I and is truncated at the ionization threshold, which has been lowered by the plasma environmental effects including the free electron Coulomb screening and the space confinements for bound electronic states due to density.

When density is high, or temperature is low, enough, degeneracy cannot be ignored. For a free electron number density ρ_f (in cm^{-3}), the degenerate temperature T_d (in eV) is approximately [50]

$$T_d = \frac{1}{8}\left(\frac{3}{\pi}\right)^{2/3}\frac{h^2}{m_e k}\rho_f^{2/3} \approx 3.75\times 10^{-15}\rho_f^{2/3}. \tag{15}$$

For a typical solid-dense plasma with a free electron density of 10^{24} cm^{-3}, when temperature is comparable to or lower than 37.5 eV, degeneracy should be considered. Free electron

degeneracy can be taken into account in the Saha–Boltzmann formalism by reformulating the ionization balance in terms of the quantum mechanical grand partition function with introduction of the chemical potential μ [51]

$$\frac{N_{I+1}}{N_I} = \frac{Z_{I+1}}{Z_I} \mathrm{e}^{-(\phi_I+\mu)/kT}, \tag{16}$$

where μ is determined by the average free electron number density N_e via

$$N_e = \frac{\sqrt{2}}{\pi^2} \frac{1}{(kT)^{3/2}} \int_0^\infty \frac{x^{1/2}\,\mathrm{d}x}{\mathrm{e}^{x-\mu/kT}+1}. \tag{17}$$

For nondegenerate cases, $\mu \approx 0$, and equations (16) and (17) reduce to equations (12) and (14), respectively. However, the Coulomb interactions between free electrons are not considered by using equation (17) to determine the chemical potential μ. The Coulomb interactions between free electrons can be taken into account approximately by using an expression similar to equation (5). From equations (5)–(7), one can see that different ion-sphere sizes and chemical potentials are calculated for ions of different ionization stages in the plasma. For simplifying the numerical solving process of the Saha equation, (17) was used when the quantum degeneracy effect was considered in the calculations of ionization balance in the plasma.

In hydrodynamic calculations, Rosseland and Planck mean opacities [50, 51] are usually used. They are defined, respectively, by

$$\frac{1}{K_R} = \int_0^\infty \frac{W_R(u)\mathrm{d}u}{\kappa(u)} \tag{18}$$

and

$$K_P = \int_0^\infty [\kappa(u) - \kappa_s(u)] W_P(u)\,\mathrm{d}u, \tag{19}$$

where $u = h\nu/kT$, κ_s is the opacity of scattering. W_R and W_P are, respectively, the Rosseland integration weight function,

$$W_R(u) = \frac{15}{4\pi^4} \frac{u^4\,\mathrm{e}^{-u}}{(1-\mathrm{e}^{-u})^2}, \tag{20}$$

and the Planck integration weight function,

$$W_P(u) = \frac{15}{\pi^4} \frac{u^3\,\mathrm{e}^{-u}}{(1-\mathrm{e}^{-u})}. \tag{21}$$

Although the process of summing atomic radiative absorption cross sections to generate opacity is similar to our early study [6], the models of the atomic structure and radiative process and the details in calculation and code are completely different from those used before.

3. Results and discussions

The opacity of hot and solid-dense plasmas requires large amounts of environmental-dependent atomic data, and the accuracy of the opacity strongly depends on the accurate atomic data. Therefore, we first discuss the environmental-dependent atomic data in section 3.1. Then, emphases will be placed on the calculation of radiative opacity in section 3.2.

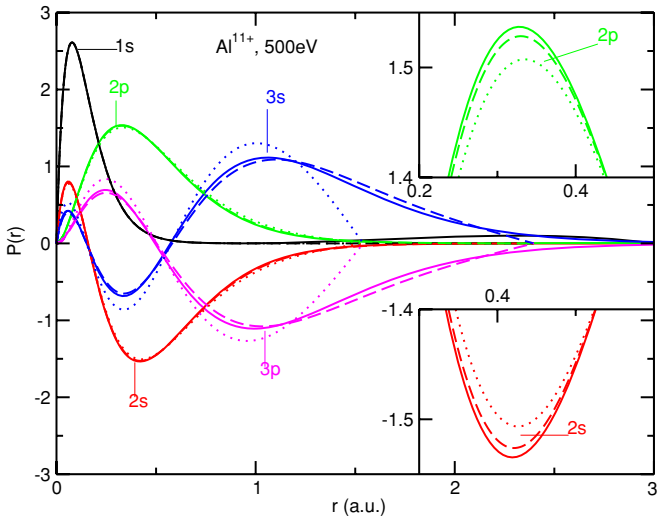

Figure 1. Density dependence of the lowest few orbitals for ion AlXII at a temperature of 500 eV, where the solid, dash and dot lines refer to the results of free ions and the ions in a plasma with a density of 5 and of 20 g cm^{-3}, respectively.

3.1. Atomic data temperature and density dependence

Correlation plays an important role in the calculation of the atomic structure. In the present study, large scale configuration interactions (CI) are involved in the calculations of energy levels and transition probabilities. Configurations of the single-, double- and triple-electron excitations to valence orbitals from the ground configuration have been included in the CI expansions. AlXII will be taken as an example to discuss the calculated results, and it will also be shown in the following section that AlXII is one of the main species in the plasma conditions discussed in the present study.

In table 1, the energy levels that belong to 1s2s and 1s2p configurations are listed. The NIST [52] recommended data for free ions are also included for comparison. A good agreement between the NIST data and the present results for free ions ensures the accuracy of the numerical calculations. To show the relative changes for energy levels, the ground state is set to zero for all densities and temperatures. Two distinct changes can be seen from table 1. First, the plasma environment influence can change the order of the energy levels. One can see that the fifth excited state of $[1s_{1/2}, 2s_{1/2}]_0$ becomes the second excited state when the density is up to 10 g cm^{-3}, due to a more significant influence on the 2p orbital than on the 2s orbital. Second, the 1s^2–1s2p transition array moves to lower photon energies resulting in a red shift of about 15 eV at a density of 20 g cm^{-3}, while the 1s2s–1s2p transition array moves to higher photon energies resulting in a blue shift of about 4 eV at the same density. Spectra changes will be seen clearly in figure 7, in which absorption peaks with a few different densities are plotted at the same temperature of 400 eV.

The energy level as well as the line shifts can be explained in terms of the ionized electron screening and the quantum confinement for bound state orbitals. Environmental-dependent distortions of a few lowest orbitals are shown in figure 1. For free ions, the outer shell orbitals have a trend to

Table 1. Energy levels (eV) for free ion AlXII along with the corresponding recommended values from NIST Database [52] and the energy level shifts (eV) of AlXII in plasmas with different temperatures kT (in eV) and densities ρ (in g cm^{-3}). The lowest levels at different plasma conditions are set to zero.

	ρ						
	0	0	0.2	1	5	10	20
	Present	NIST			ΔE		
$1s^2$	0	0			$kT = 300$ eV		
$[1s_{1/2}, 2s_{1/2}]_1$	1575.72	1574.98	−0.697	−1.833	−6.067	−10.803	−18.725
$[1s_{1/2}, 2p_{1/2}]_0$	1588.36	1587.97	−0.621	−1.584	−4.936	−8.630	−14.835
$[1s_{1/2}, 2p_{1/2}]_1$	1588.68	1588.12	−0.622	−1.585	−4.941	−8.640	−14.854
$[1s_{1/2}, 2p_{3/2}]_2$	1589.39	1588.76	−0.622	−1.588	−4.954	−8.664	−14.897
$[1s_{1/2}, 2s_{1/2}]_0$	1589.68	1588.95	−0.703	−1.862	−6.248	−11.184	−19.405
$[1s_{1/2}, 2p_{3/2}]_1$	1599.38	1598.29	−0.633	−1.610	−5.063	−8.923	−15.339
					$kT = 400$ eV		
$[1s_{1/2}, 2s_{1/2}]_1$			−0.692	−1.816	−5.981	−10.533	−18.548
$[1s_{1/2}, 2p_{1/2}]_0$			−0.628	−1.572	−4.865	−8.410	−14.680
$[1s_{1/2}, 2p_{1/2}]_1$			−0.629	−1.574	−4.871	−8.420	−14.700
$[1s_{1/2}, 2p_{3/2}]_2$			−0.630	−1.577	−4.883	−8.443	−14.745
$[1s_{1/2}, 2s_{1/2}]_0$			−0.695	−1.844	−6.160	−10.907	−19.222
$[1s_{1/2}, 2p_{3/2}]_1$			−0.636	−1.597	−4.991	−8.696	−15.182
					$kT = 500$ eV		
$[1s_{1/2}, 2s_{1/2}]_1$			−0.680	−1.792	−5.942	−10.455	−18.484
$[1s_{1/2}, 2p_{1/2}]_0$			−0.621	−1.557	−4.833	−8.340	−14.623
$[1s_{1/2}, 2p_{1/2}]_1$			−0.621	−1.558	−4.838	−8.350	−14.639
$[1s_{1/2}, 2p_{3/2}]_2$			−0.622	−1.561	−4.851	−8.374	−14.677
$[1s_{1/2}, 2s_{1/2}]_0$			−0.683	−1.819	−6.121	−10.830	−19.155
$[1s_{1/2}, 2p_{3/2}]_1$			−0.628	−1.581	−4.958	−8.628	−15.116

move to the outer region of the ion-sphere because of Pauli principle and the repulsions between electrons. In dense matter, however, the outer shell orbitals move back to the inner region of the ion sphere due to the interaction with neighbouring ions. At the same time, there are a lot of ionized electrons distributed in the inner region of the sphere. Both ionized electron screening and quantum confinement move an energy level to higher energies. However, in an atomic potential dominated by the nuclear Coulomb attraction, the strength of these two effects is different for inner and outer shell orbitals. As the ionized electrons concentrated around the nuclei, the up shifts of the inner shell orbital energy caused by screening are usually larger than those of the outer shell orbital energy. In contrast, the up shifts of the orbital energy caused by quantum confinement are larger for outer shells than for inner shells. The blue and red shifts of the transition lines are results of the difference between the energy levels shifts of initial and final states. The up shift of the 1s orbital energy caused mainly by screening is larger than that of 2p orbital energy caused by both screening and quantum confinement so that the $1s^2$–1s2p transition array displays red shift with increase of the density. The screening effects are nearly the same for 2s and 2p orbitals, while the quantum confinement effect for the 2p orbital is stronger than that for the 2s orbital, as the 2s wavefunction has more nodes than 2p. So, the 1s2s–1s2p transition array displays blue shift with increase of the density.

The distortions of orbitals induce changes of oscillator strengths and ionization potential depression as well. Figure 2 shows the changes of oscillator strengths of AlXII along

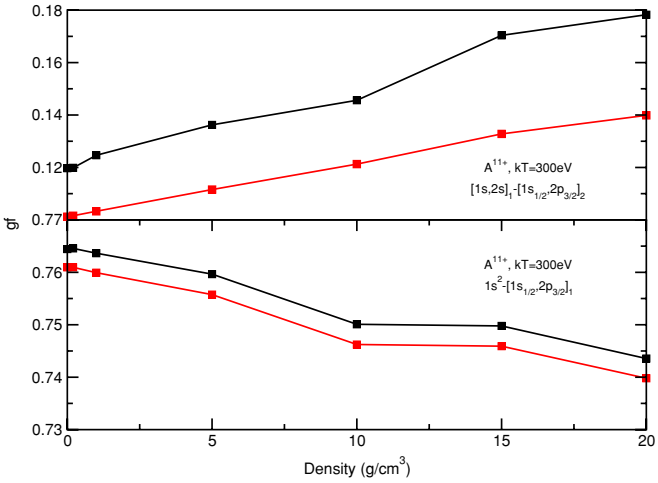

Figure 2. Changes of the oscillator strengths of 1s–2p and 2s–2p transitions for ion AlXII as a function of density at a temperature of 300 eV.

with the plasma parameter. The oscillator strength of the $[1s, 2s]_1$–$[1s_{1/2}, 2p_{3/2}]_2$ transition becomes larger along with the density increase due to the more overlap between the two orbitals of 2s and 2p, while the oscillator strength of the $1s^2$–$[1s_{1/2}, 2p_{3/2}]_1$ transition decreases with the density at 300 eV because of the less overlap between the orbitals of 1s and 2p at higher densities. Although the 2p wavefunction around the maximum point moves outside slightly with density, it induces changes of the oscillator strength apparently because the 1s

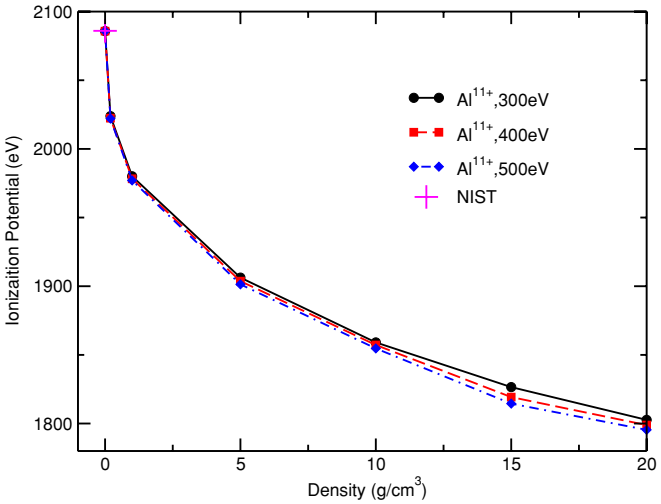

Figure 3. Ionization potential depression with density at a few temperatures.

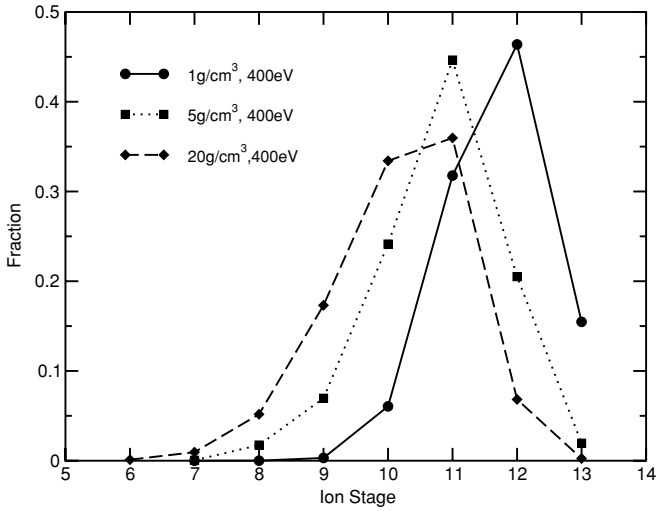

Figure 4. Charge state fractions in the Al plasma at a temperature of 400 eV and three densities.

wavefunction decays very fast in this region. It is apparent that the plasma environment introduces the rearrangement of transition probabilities among different transition arrays and eventually influences the opacity of the plasma.

Figure 3 plots the depression of the ionization potential for AlXII with density. The ionization potential decreases rapidly with the increase of density. The highly excited orbitals are easily ionized to free electron states in the plasmas. For instance, when the density gets to 5 g cm^{-3}, the ionization potential depresses nearly 200 eV compared to the free ion, while it depresses only 100 eV more, when the density is up to 20 g cm^{-3} from 5 g cm^{-3}. The tightly bound orbitals of $n = 2, 3$ are not easy to ionize to free ones, even with the density up to nearly ten times of solid density. The cutoff of bound states in the calculation of the partition function of the ions, which is very essential for the calculation of charge state abundance through solving the Saha equation, is determined by the ionization potential. So, how well evaluated ionization potentials of ions in dense plasmas eventually influence the total opacity through the charge state fraction. An ionization potential of 2085.71 eV was obtained in the present calculation for free AlXII ion very close to the NIST recommended value of 2085.98 eV [52].

All other ions existing in the plasma are calculated in the same way as done for AlXII and are included in the ionization balance calculation and opacity calculation discussed in the following section.

3.2. Radiative opacity of hot and solid-dense aluminium plasma

Figure 4 plots the charge state abundance in different plasma conditions. At 400 eV, the average charge states are 11.7, 10.5 and 10.2 for densities of 1, 5 and 20 g cm^{-3}, respectively. AlXII is one of the main species in these cases, so, AlXII will be taken as an example to show the environmental dependence of ion spectra in plasmas. Figure 5 shows the changes of plasma average ionization degree along with density at a

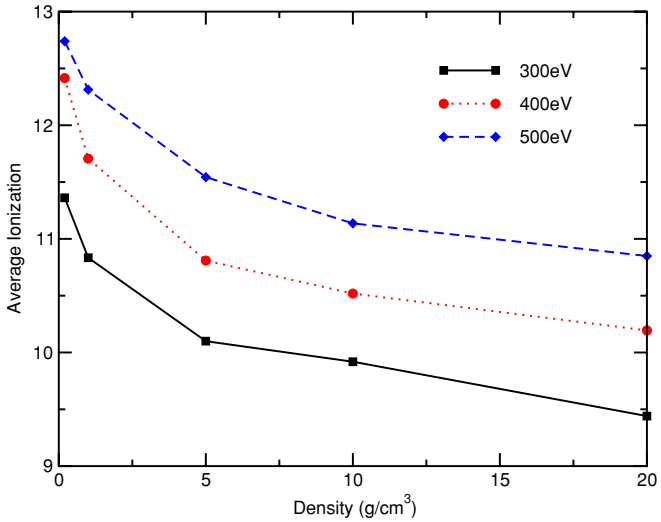

Figure 5. Dependence of mean ionization degree of Al plasma on density at three temperatures.

few different temperatures. At lower density and higher temperature, the highly excited and valence orbitals can be ionized to free ones due to the thermoionization. With increase of density, recombination of ionized electrons increases and reduces the average ionization degree. For example, At 0.2 g cm^{-3} and 400 eV, the average ionization degree is 12.5, however, when the density is up to 20 g cm^{-3}, the average ionization degree decreases to 11.1, and almost one and a half electrons are compressed back to bound states. On the other hand, when the density is above a certain value some of the highly excited states become ionized states due to the interactions between electrons in neighbouring atoms and cause the so-called pressure depression of the ionization potential. Take the same example, it will be seen in figure 7 that all the absorption peaks above 1750 eV disappear in the spectra of 20 g cm^{-3} due to the depression of the ionization potential. So, the recombination of ionized electrons with density increase occurs mainly on the low-lying states of the

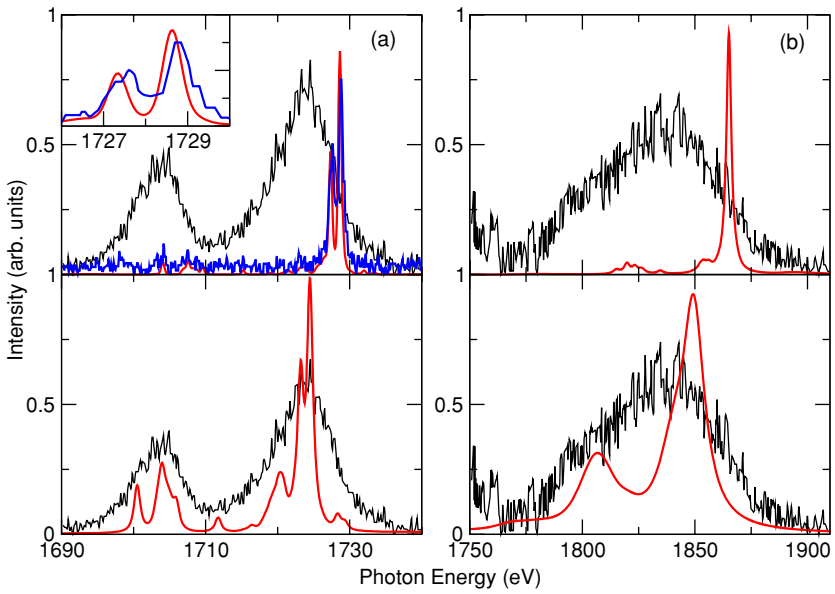

Figure 6. Comparisons of (a), the Lyα and its He-like satellites, and (b), the Heβ and its satellites, between the present model (red solid lines) and experimental data (black and blue solid lines) of Saemann *et al* [13]. The present results of (300 eV, 1 g cm^{-3}, Ne $\approx 2.4 \times 10^{23}$) and (300 eV, 5 g cm^{-3}, Ne $\approx 1.1 \times 10^{24}$) are plotted in the top and bottom parts of the figure, respectively. In the inset of the top part of (a), the blue line shows the experimental result of the so-called low-density plasma.

ions. It is expected that average charge increases again at higher density due to competition between the recombination and the pressure ionizing processes. It can be estimated that the ionized electron number density at 20 g cm^{-3} and 300 eV is approximately 5×10^{24} cm^{-3}, and according to equation (15), the degeneracy temperature is about 100 eV well below 300 eV. Therefore, the quantum degeneracy effect in the present temperature and density region is not very considerable. From the highest bound orbital radius below the ionization threshold, it can be estimated that the Coulomb interaction energy E_c between an ion and a near threshold ionized electron is approximately $|E_c| \approx 100$ eV at 20 g cm^{-3} and 300 eV and $|E_c| \approx 50$ eV at 1 g cm^{-3} and 300 eV. The average interaction potential energy between two electrons is about one order less than $|E_c|$. Therefore, neglect of $|E_c|$ when solving the Saha equation could induce non-negligible errors that must be corrected in further studies if the density is up to 20 g cm^{-3}.

Comparisons with experiments are made and shown in figure 6. Only a few experimental results were reported in the literature on the emission and absorption spectra of Al plasma [12, 13] in the density and temperature range of the present study. The experimentalists [13] gave detailed emission spectra including line broadening and shift around Heβ, Lyα, and their Li and He like satellite transition lines. The free electron number density and temperature in the experiment were estimated to be 5–10 $\times 10^{23}$ and 300 eV, respectively. Comparisons are made between the present (300 eV, 1 g cm^{-3}, Ne $\approx 2.4 \times 10^{23}$) and (300 eV, 5 g cm^{-3}, Ne $\approx 1.1 \times 10^{24}$) results and experimental data. Because relative intensity was obtained in the experiment, in order to make the comparison, the continuum background in the experimental data was subtracted and the present results of bound–bound transitions are normalized according to the experimental data. Broadening and shift of the Lyα line provide information about the electron density. The experimental data include both the so-called low-density and high-density data. Dependence of the line broadening and shift on the density was demonstrated clearly by the experiment. As the strength and position of the free hydrogen-like Lyα transition have been well known without uncertainties in both theory and experiment, the comparison between theory and experiment for plasma spectra can give direct examination on the theoretical treatment about plasma effect and can also give estimation about the plasma parameters. In the top part of figure 6(a), one can find that position, broadening and strength of the experimental low-density Lyα line are reproduced very well by the present (300 eV, 1 g cm^{-3}, Ne $\approx 2.4 \times 10^{23}$) calculation. Theory gives a 0.3 eV red shift compared to the free ion Lyα line. From the top part of figures 6(a) and (b), it can be seen that the red shifts and broadening of the experimental high-density spectra are apparently larger than the present (300 eV, 1 g cm^{-3}, Ne $\approx 2.4 \times 10^{23}$) calculation. From the bottom part of figures 6(a) and (b), one can see that the red shifts of the experimental spectra are well predicted by the present (300 eV, 5 g cm^{-3}, Ne $\approx 1.1 \times 10^{24}$) calculation, while the broadening was underestimated by theory. There might be two main reasons responsible to the line broadening difference between theory and experiment. The first one is that the ion–ion dynamical interactions are not included in the present model. The second one is that there may be electron density nonuniformity in the experiment, which induces the overlap of the spectra with different red shifts resulting in a broader spectrum.

Figure 7 plots the calculated spectrally resolved opacity with comparisons between the present and the AA models.

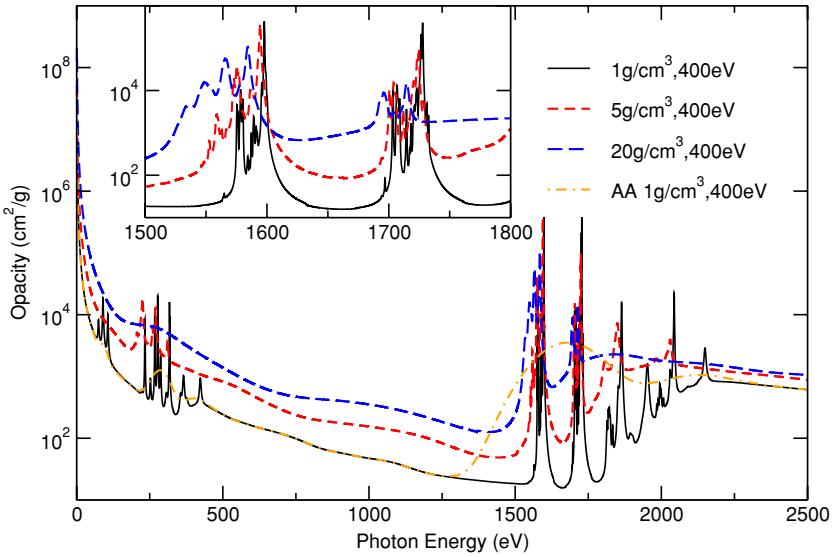

Figure 7. Density dependence of radiative opacity of Al plasma at a temperature of 400 eV.

Taking the case of 1 g cm^{-3} and 400 eV as an example, fine splits in the spectra and detailed information about the transitions can be found from the results of the present DLA model. The absorption structures in the photon energy range of 1565–1599 eV and 1695–1750 eV are dominated by 1s–2p transitions. These absorption structures split into two groups: the first one is due to the transitions from the ground configuration and the second one is due to the satellite lines caused by the transitions from 1s2s and 1s2p excited configurations. The absorption around 1863 eV is due to 1s–3p transitions. The peak nearby 1950 eV is due to the absorption of 1s–4p transitions. The absorption above 2030 eV is mainly attributed to the satellite lines caused by transitions of one electron from 1s orbital to 3p or 4p orbitals from 1s2s and 1s2p excited configurations. The absorption around 270 eV is mainly made by the L-shell transitions. The M-shell transitions dominated the contributions near 140 eV. More detailed information about the atomic processes can be obtained from the DTA/DLA model. For example, the two fine absorption peaks between 1700 eV and 1725 eV correspond to the satellite lines of 1s2s–2s2p and 1s2p–2p^2 transitions. The final states of these kinds of satellite transitions locate well above the ionization states and can autoionize to 1sϵl states. It can also be seen as well that the average atom model predicts the line broadening of the absorption peak around 1600 eV being more than 400 eV at the present plasma conditions, which is much larger than the value of only about 50 eV predicted by the present DLA model for the resonance transitions from 1s to 2p orbitals contributed by all the ion species. Experiments [11, 13] showed that the line broadening of the corresponding absorption in the hot and solid-dense Al plasmas is no more than 30 eV. It can be concluded that line broadening is overestimated considerably by the AA model for the present hot and solid-dense aluminium plasmas.

Figure 7 shows also changes of the calculated opacities with three densities of 1, 5 and 20 g cm^{-3}. Taking the absorptions in 1550–1598 eV and 1685–1725 eV as examples, these two absorption peaks are broadened and become stronger along with the density. Although the absorptions of AlXIII around 1710 eV decrease with the decrease of its abundance, the contributions of AlXII, AlXI and AlX increase much more and merged together in the range of 1550–1597 eV and 1685–1750 eV. Because of the strengthening of collision among ions and electrons as a function of the matter density, the electron impact broadening becomes a dominant one in all the broadening mechanisms and dominates the line shape function such as the Voigt Profile and the widths of the spectral lines. So the total absorptions nearby the two peaks increase and are broadened as well with the density. With the increase of density, the line shift is apparent, and the two corresponding peaks shift their maximum to lower photon energy. For examples, the resonance transition from 1s to 2p locates at 1598.8, 1594.4 and 1584.2 eV for the case of 1, 5 and 20 g cm^{-3}, respectively. Some absorption peaks related to high-lying excited states disappear gradually with increase of density, because of the ionization potential depression. Generally, more complex ions have more energy levels and more transition lines. So, even though one cannot say definitely the difference for each transition rate of different ions, in total, the more complex the ion is, the stronger the total absorption and emission. On the basis of this fact, one can understand the increase of the total absorption strength along with the increase of density because more complex ions exist in dense plasmas as shown in figure 4 before pressure induced ionization occurs. For the same reason, one can understand the temperature dependence of the total opacity shown next in figure 8.

Figure 8 shows the changes of spectrally resolved opacity with temperatures. When density is chosen, with increase of temperature, the absorption lines from the K-shell around 1995 eV and L-shell around 270 eV move to higher photon energies. There are two reasons responsible for this trend of line shift. First, at a higher temperature, the localized ionized electrons have larger kinetic energies to move to

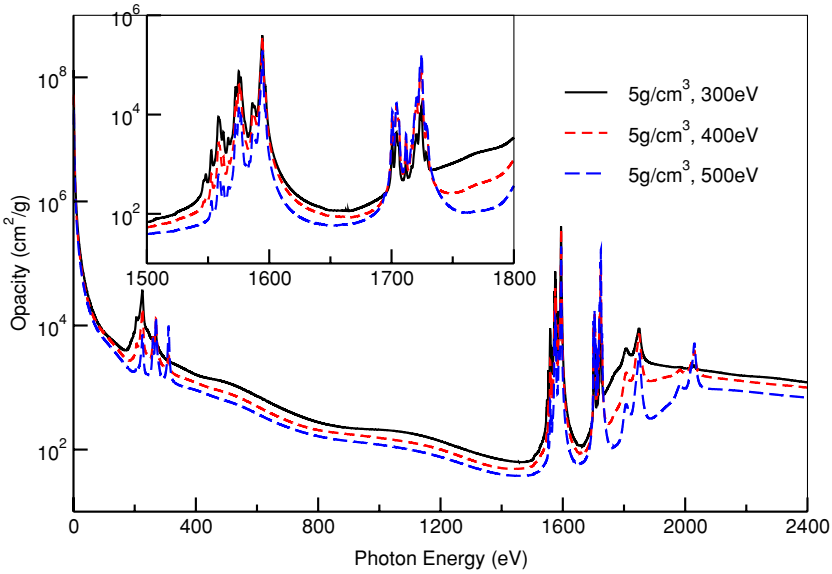

Figure 8. Temperature dependence of radiative opacity of Al plasma at a density of 5 g cm^{-3}.

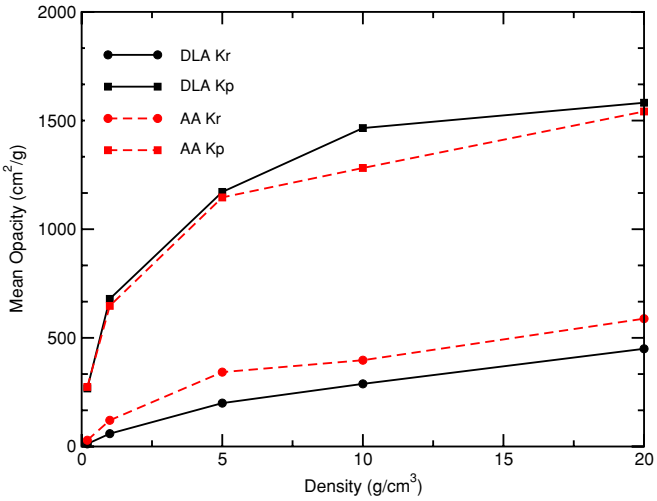

Figure 9. Comparisons of the radiative Rosseland and Planck mean opacity of Al plasma at a temperature of $kT = 400$ eV between the present results (DLA) and those of the AA model.

the outer region of the ion-sphere and make the screening effect of ionized electrons smaller. As a result, the role of quantum confinement becomes more important compared to the screening effect. As mentioned above, the quantum confinement effect is generally stronger for higher lying states, so that spectral lines move to higher photon energies with increase of temperature. Second, the mean ionization degree increases with temperature. For instance, the average ionization degrees are 10.1, 10.8 and 11.5 for temperatures of 300 eV, 400 eV and 500 eV, respectively, when density is 5 g cm^{-3}. The corresponding maximum fractions of the ion are AlXI (41%), AlXII (44.6%) and AXIII (41%), respectively. The changes of main species make the absorption lines around 1995 and 270 eV move to a higher photon energy as well.

Planck and Rosseland mean opacities are also calculated and compared with the AA model in figure 9. It is well known that the Rosseland mean opacity depends sensitively on the depth of the transmission windows of the spectrum, while the Planck mean opacity is determined mainly by the strengths of absorption peaks. The Planck mean opacity is not quite sensitive to the line shapes, while the Rosseland mean opacity strongly depends on the line shapes. Calculation of line broadening using full quantum theory is so complex that it is not applicable for the line-by-line simulation of hot and dense plasmas. In many cases, one usually uses simplified formulae based on empirical or semi-empirical approximations [48] for the electron impact-induced line profile. So, more differences among different models are usually found for Rosseland mean opacity. Big differences for Planck mean opacity are only found when uncertainties are involved in the accounting of total transitions. The Planck mean opacities of the DTA/DLA model are in good agreement with the results of the AA model at a density of 0.2, 1, 5 and 20 g cm^{-3}. While, the Rosseland mean opacities of the DTA/DLA model are systematically smaller than the results of the AA model. In the present DTA/DLA model, CI calculations to optimize the true atomic energy levels are carried out. The method is more close to the actual transition, and higher accuracy of mean opacity can be obtained from it. The most important source for the difference of Rosseland mean opacity between DTA/DLA and AA models is the overestimated line broadening used in the AA model, which fill fully the transmission windows between the transition arrays.

4. Conclusion

In conclusion, a self-consistent approach combining a modified MCDF scheme for bound electrons with the ionized electron screening and a proper consideration of ionization balance in the plasma has been developed to make an accurate calculation for radiative opacity of hot and solid-dense plasmas. To validate this DTA/DLA model and study the influence of the plasma environment on the opacity,

spectrally resolved radiative opacity and Rosseland and Planck means opacities are calculated. Results demonstrate that the 1s–2p transition array moves to low photon energies with plasma density, leading to a red shift of the corresponding absorption peaks. The ionization potential of ion species in the plasma depresses with the density and the oscillator strengths of the bound–bound transitions changes as well. All the environmental-dependent atomic data have a significant influence on the charge state fraction and spectrally resolved opacity. Comparisons between the results of the present model, the AA model and the existing experiments are made to show that the environment effect as well as accurate line-by-line accounting is essential for description of the radiative properties of hot and solid-dense plasmas.

Acknowledgments

This work was supported by the National Natural Science Foundation of China under grant nos. 10734140 and 60621003, the National Basic Research Program of China (973 Program) under grant no. 2007CB815105, and the National High-Tech ICF Committee in China.

References

[1] Rogers F J and Iglesias C A 1994 *Science* **263** 50
Iglesias C A, Wilson B G, Rodgers F J, Goldstein W H, Bar-Shalom A and Oreg J 1995 *Astrophys. J.* **445** 855
Rozsnyai B F 2001 *J. Quant. Spectrosc. Radiat. Transfer* **71** 655
[2] Storm E 1988 *J. Fusion Energy* **7** 131
[3] Seaton M J 1987 *J. Phys. B: At. Mol. Phys.* **20** 6363
The Opacity Project Team *The Opacity Project* vols I and II (Bristol: Institute of Physics Publishing)
[4] Iglesias C A and Rogers F J 1996 *Astrophys J.* **464** 943
Iglesias C A, Chen M H, Sonnad V and Wilson B G 2003 *J. Quant. Spectrosc. Radiat. Transfer* **81** 227
[5] Hakel P, Sherrill M E, Mazevet S, Abdallah J Jr, Colgan J, Kilcrease D P, Magee N H, Fontes C J and Zhang H L 2006 *J. Quant. Spectrosc. Radiat. Transfer* **99** 265
[6] Zeng J L, Jin F T, Yuan J M, Lu Q S and Sun Y S 2000 *Phys. Rev.* E **62** 7251
Zeng J L, Yuan J M and Lu Q S 2001 *Phys. Rev.* E **64** 066412
Gao C and Zeng J L 2008 *Phys. Rev.* E **78** 046407
[7] Bailey J *et al* 2007 *Phys. Rev. Lett.* **99** 265002
[8] Rickert A 1995 *J. Quant. Spectrosc. Radiat. Transfer* **54** 325
[9] Yaakobi B, Skupsky S, McCrory R L, Hooper C F, Deckman H, Bourke P and Soures J M 1980 *Phys. Rev. Lett.* **44** 1072
[10] Rousse A, Audebert P, Geindre J P, Falliés F, Gauthier J C, Mysyrowicz A, Grillon G and Antonetti A 1994 *Phys. Rev.* E **50** 2200
[11] Peyrusse O, Busquet M, Kieffer J C, Jiang Z and Côté C Y 1995 *Phys. Rev. Lett.* **75** 3862
[12] Leboucher-Dalimiera E, Sauvanb P, Angeloa P, Poqu4erussea A, Schotta R, Dufoura E, Minguezb E and Calistic A 2001 *J. Quant. Spectrosc. Radiat. Transfer* **71** 493
Schott R *et al* 2003 *J. Quant. Spectrosc. Radiat. Transfer* **81** 441
[13] Saemann A, Eidmann K, Golovkin I E, Mancini R C, Andersson E, Förster E and Witte K 1999 *Phys. Rev. Lett.* **82** 4843
[14] Glenzer S H, Gregori G, Rogers F J, Froula D H, Pollaine S W, Wallace R S and Landen O L 2003 *Phys. Plasmas* **10** 2433
[15] Dobosz S, Doumy G, Stabile H, D'Oliveira P, Monot P, Réau F, Hüller S and Martin P 2005 *Phys. Rev. Lett.* **95** 025001
[16] Sandhu A S, Kumar G R, Sengupta S, Das A and Kaw P K 2006 *Phys. Rev.* E **73** 036409
[17] Edwards M H *et al* 1996 *Phys. Rev. Lett.* **97** 035001
[18] Chen S N *et al* 2007 *Phys. Plasmas* **14** 102701
[19] Moses E I, Boyd R N, Remington B A, Keane C J and Al Ayat R 2009 *Phys. Plasmas* **16** 041006
[20] Bailey J E, Rochau G A, Mancini R C, Iglesias C A, MacFarlane J J, Golovkin I E, Blancard C, Cosse P and Faussurier G 2009 *Phys. Plasmas* **16** 058101
[21] Hakel P, Mancini R C, Andiel U, Eidmann K, Pisani F, Junkel-Vives G and Abdallah J 2009 *High Energy Density Phys.* **5** 35
[22] Rozsnyai B F 1972 *Phys. Rev.* A **5** 1137
Rozsnyai B F 1982 *J. Quant. Spectrosc. Radiat. Transfer* **27** 211
Rozsnyai B F 1991 *Phys. Rev.* A **43** 3035
[23] Liberman D A 1979 *Phys. Rev.* A **20** 4981
[24] Crowley B J B and Harris J W O 2001 *J. Quant. Spectrosc. Radiat. Transfer* **71** 257
[25] Yuan J M 2002 *Phys. Rev.* E **66** 047401
[26] Bar-Shaloma A, Oreg J, Goldstein W H, Shvarts D and Zigler A 1989 *Phys. Rev.* A **40** 3183
Bar-Shaloma A, Oreg J and Klapisch M 2006 *J. Quant. Spectrosc. Radiat. Transfer* **99** 35
Barshalom A and Oreg J 2007 *High Energy Density Phys.* **3** 12
[27] Pain J C, Dejonghe G and Blenski T 2006 *J. Quant. Spectrosc. Radiat. Transfer* **99** 451
[28] Bauche-Arnoult C, Bauche J and Klapisch M 1978 *J. Opt. Soc. Am.* **68** 1136
[29] Debye P and Hückel E 1923 *Phys. Z.* **24** 185
[30] Stewart J C and Pyatt K D 1966 *Astrophys. J.* **144** 1203
[31] Skupsky S 1980 *Phys. Rev.* A **21** 1316
[32] Dharma-Wardana M W C and Perrot F 1982 *Phys. Rev.* A **26** 2096
[33] Ichimaru S 1982 *Rev. Mod. Phys.* **54** 1017
[34] Nguyen H, Koening M, Benredjem D, Caby M and Coulaud G 1986 *Phys. Rev.* A **33** 1279
[35] Crowley B J B 1990 *Phys. Rev.* A **41** 2179
[36] Murillo M S and Weisheit J C 1998 *Phys. Rep.* **302** 1
[37] Al Kuzee J, Hall T A and Frey H D 1998 *Phys. Rev.* E **57** 7060
[38] Gauthier G B, Rose S J, Sauvan P, Angelo P, Leboucher-Dalimier E, Calisti A and Talin B 1998 *Phys. Rev.* E **58** 942
[39] Mossé C, Calisti A, Stamm R, Talin B, Lee R and Klein L 1999 *Phys. Rev.* A **60** 1005
[40] Junkel G C, Gunderson M A and Hooper C F Jr 2000 *Phys. Rev.* E **62** 5548
[41] Saha B and Fritzsche S 2007 *J. Phys. B: At. Mol. Opt. Phys.* **40** 259
[42] Li Y Q, Wu J, Hou Y and Yuan J M 2008 *J. Phys. B: At. Mol. Opt. Phys.* **41** 145002
[43] Mínguez E *et al* 2003 *J. Quant. Spectrosc. Radiat. Transfer* **81** 301
[44] Meng C S, Zhao Z X and Yuan J M 2008 *Chin. Phys. Lett.* **25** 2452
Hou Y and Yuan J M 2009 *Phys. Rev.* E **79** 016402
[45] Grant I P 1984 *Int. J. Quantum Chem.* **25** 23
[46] Dyall K G, Grant I P, Johnson C T, Parpia F A and Plummer E P 1989 *Comput. Phys. Commun.* **55** 425
[47] Thomas L H 1927 *Proc. Camb. Phil. Soc.* **23** 542
Fermi E 1928 *Z. Phys.* **48** 73
[48] Dimitrijevic M S and Konjevic N 1980 *J. Quant. Spectrosc. Radiat. Transfer* **24** 451
Dimitrijevic M S and Konjevic N 1987 *Astron. Astrophys.* **172** 345

[49] Saha M N 1920 *Phil. Mag.* **40** 472
Saha M N 1921 *Proc. R. Soc. London* A **99** 135

[50] Zel'dovich Ya B and Raizer Yu P 1966 *Physics of Shock Waves and High-Temperature Hydrodynamics Phenomena* vol I (New York: Academic)

[51] Xu X S and Zhang W X 1986 *Introduction to Practical Theory of EOS* (Beijing: Science Press) (in Chinese)

[52] Ralchenko Yu, Kramida A E and Reader J and NIST ASD Team 2008 *NIST Atomic Spectra Database* version 3.1.5 (Gaithersburg, MD: National Institute of Standards and Technology) http://physics.nist.gov/asd3